Journal of Molecular Catalysis A: Chemical 395 (2014) 251–260

Contents lists available at ScienceDirect

Journal of Molecular Catalysis A: Chemical

journal homepage: www.elsevier.com/locate/molcata

Role of basicity, calcinations, catalytic activity and recyclability of hydrotalcite in eco-friendly synthesis of coumarin derivatives

Pramod K. Sahu[a,b,*], Praveen K. Sahu[b,**], Dau D. Agarwal[a,b]

[a] School of Studies in Chemistry, Jiwaji University, Gwalior 474011, Madhya Pradesh, India
[b] Department of Industrial Chemistry, Jiwaji University, Gwalior 474011, Madhya Pradesh, India

ARTICLE INFO

Article history:
Received 19 May 2014
Received in revised form 12 July 2014
Accepted 14 July 2014
Available online 24 July 2014

Keywords:
Calcination
Catalytic activity
Aging
Reusability
Coumarin derivatives

ABSTRACT

An efficient and simple protocol is described for synthesis of coumarin derivatives using Mg–Al-CO_3 and Ca–Al-CO_3 hydrotalcite as an environmental friendly and reusable heterogeneous catalyst under solvent free conditions. The catalysts were characterized by Hammett titration, SEM and XRD data. Present study revealed that catalytic activity and basicity depend on compositions of hydrotalcite. The calcined hydrotalcite with an Mg/Al of 3:1 derived from calcinations at 750 K was found to be suitable catalyst that gives the highest basicity and the best catalytic activity for this reaction. Catalyst allows short reaction time, high catalytic activity, easy to work up and is reusable. Step economy, atom efficiency and solvent free conditions are some important salient features of this protocol.

1. Introduction

Coumarins (chomene-2-ones, benzopyran-2-ones) are naturally occurring classes of compound, which having variety of pharmacological activity dependent on the substitution patterns [1]. Coumarins core structure represents a highly privileged and biologically relevant molecular scaffold which occurs in many natural products. For example, autumnariol has been isolated from onions of *Eucomis autumnalis* Greab (Liliaceae) [2]. A number of related natural products, such as autumnariniol [3], alternariol [4], and altenuisol [5], have been isolated (Fig. 1) [6]. Recently several synthetic procedures for the preparation of coumarin derivatives have been reported using montmorillonite K-10 [7], zinc [8], indium (III) chloride [9], $TiCl_4$ [10], $ZrCl_4$ [11], sulfated zirconia [12], Lewis acidic chloroaluminate ionic liquid [13], bismuth nitrate [14], Wells–Dawson heteropolyacid [15], samarium (III) [16], PIDA/I_2-mediated [17], $InCl_3$ [18], $HClO_4$·SiO_2 [19], DMAP and Et_3N [20]. Literature survey demonstrated that reported methods have suffered drawbacks such as low yield, long duration, and used hazardous solvent such as organic solvent as compared to water, not reusable, higher catalyst loading, and relatively higher temperature conditions.

The drawback of ionic liquids is that it cannot be removed by distillation and their limited solubility in water restricts their use. They have high cost and also acute toxicity for aquatic organism and human [21]. Hydrotalcites (HTs) are synthetic or natural layered materials made of positively charged two-dimensional sheets of mixed hydroxides with water and exchangeable charge-compensating anions [22]. Hydrotalcites are increasingly regarded as a good alternative to the traditional homogenous base catalysts such as NaOH and KOH for several base-catalyzed reactions that are important for the pharmaceutical and fragrance industries [23]. A well-documented example is the isomerization of eugenol and safrole [24]. As far as green chemistry is concerned, hydrotalcites offer several advantages over these corrosive, dissolved catalysts, easy separation from the reaction mixture, recycling possibilities, decreased corrosion of the reactor, so forth [25]. The range of applications of hydrotalcite base materials is virtually unlimited. Hydrotalcites can be involved in the preparation of catalysts dedicated to the production of H_2 [26], wide range of organic compounds [27] and production of biodiesel by transesterification of triglycerides with methanol [28]. In addition to the above numerous experimental investigations have been published on the use of hydrotalcites for catalytic applications [29]. In present communication, we have used hydrotalcite as catalyst led to formation of high yield of coumarin derivatives under solvent free conditions.

* Corresponding author at: School of Studies in Chemistry, Jiwaji University, Gwalior 474011, Madhya Pradesh, India. Tel.: +91 9993932425.
** Corresponding author. Tel.: +91 9993932425.
E-mail addresses: sahu.chemistry@gmail.com, researchdata6@gmail.com (P.K. Sahu), praveensahu1234@gmail.com (P.K. Sahu).

http://dx.doi.org/10.1016/j.molcata.2014.07.024
1381-1169/

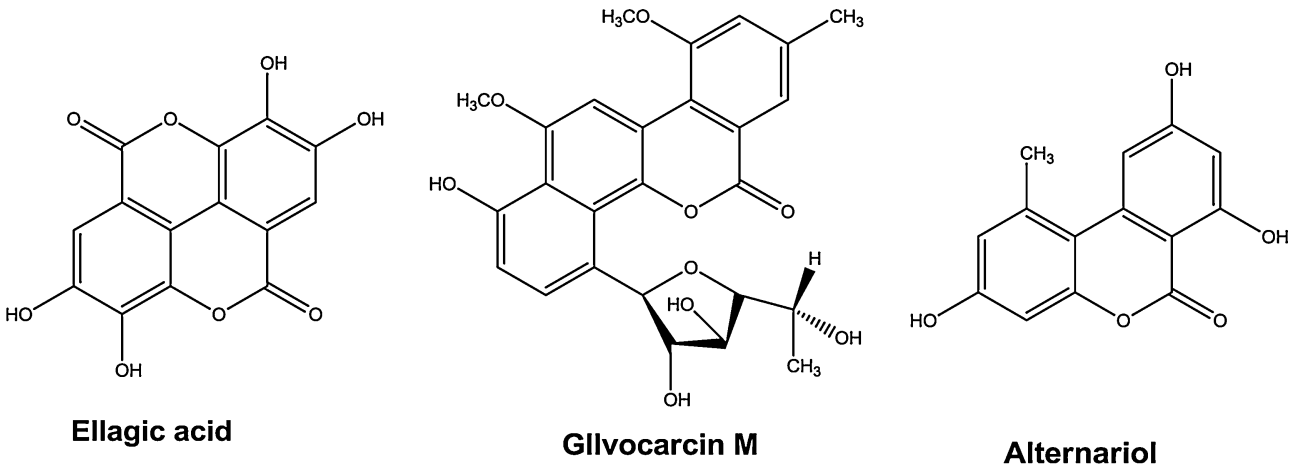

Fig. 1. Natural occurring products with coumarins core.

Table 1
Optimization of hydrotalcite as a catalyst (Mg–Al-HT (Mg/Al = 3)).

Entry	Catalyst loading (mg)	Time (min)	Yield (%)
1	10	120	52
2	20	90	74
3	50	30	97
4	75	30	97
5	100	30	96

2. Results and discussion

In order to evaluate the appropriate catalyst loading, a model reaction of resorcinol (0.0025 mol) and ethyl acetoacetate (0.0025 mol) were carried out using 10 mg, 20 mg, 50 mg, 80 mg, and 100 mg of hydrotalcite as catalyst at 70 °C. The catalyst loading 50 mg was found to be the optimal quantity (Table 1). Catalyst was reused and the results show that the hydrotalcite (Mg–Al-CO_3) can be reused as such without significant loss in yield (Table 2). Reusability of catalyst reduces the cost of production. The procedure was efficient and greatly reduced the role of solvent thus reducing environmental pollution. This procedure was easy to work up because after completion of the reaction, mass was cooled to room temperature and poured directly in cold water. Precipitate was form and filtered easily. Solid was dissolved in ethanol and filtered to separate hydrotalcite.

Basicity of hydrotalcite is a key for the preparation of material with high performance [30]. It can be achieved by changing the nature of M^{2+}/M^{3+} metals [31]. As far as Mg–Al mixed oxides of hydrotalcite is concerned, a correlation can be established between the composition and the basicity: when the amount of Al increases, the total number of basic sites decreases [25(a),32]. The decrease in basic site density observed in Mg–Al mixed oxide derived from hydrotalcites when increasing the Al content is reported to be the reason for decreasing activity in the Knoevenagel condensation reaction between glyceraldehydes acetonide and ethyl acetoacetate [33]. The performance of Mg–Al mixed oxide in the methanolysis of soybean oil was shown to be dependent on the Mg/Al ratio [34]. Numerous authors have tried to identify the best composition of Mg–Al mixed oxide catalysts in the case of various reaction. A set of Mg–Al hydrotalcite-like precursors with different Mg/Al atomic ratios was studied by Diez et al. [35]. The optimum Mg/Al molar ratio is dependent on the target reaction and more precisely, on the basic strength needed to activate the reactant. In order to check the basicity effect of hydrotalcite catalyst on the yield of the synthesized coumarin derivatives, hydrotalcite with different metallic ratios of Mg–Al-CO_3, Ca–Al-CO_3 and their metal oxide were tried under solvent free conditions and concluded that (3:1) Mg–Al-CO_3, (3:1) Ca–Al-CO_3 were more suited hydrotalcites to catalyze the reaction (Table 3). The results show that basicity of hydrotalcite affected the reaction time and yields of target product. Among all the metallic ratio of hydrotalcites, 3:1 ratio of hydrotalcite (Mg–Al-CO_3) gives the highest yield with lower time.

Table 2
Reusability of hydrotalcite (Mg–Al-HT, (Mg/Al = 3)).[a]

Product	Fresh HT	Reuse (I)	Reuse (II)	Reuse (III)	Reuse (IV)
1a	97	95	95	93	92

[a] Reaction conditions: resorcinol (0.0025 mol), ethyl acetoacetate (0.0025 mol), hydrotalcite (50 mg), heating at 70 °C.

2.1. Recyclability and reusability of hydrotalcite

A model reaction has been carried out using of resorcinol (0.0025 mol) and ethyl acetoacetate (0.0025 mol) for recyclability and reusability of hydrotalcite as catalyst by incorporating 50 mg of hydrotalcite catalyst. After completion of reaction, the contents were filtered to recycle the hydrotalcite catalyst through whatman filter 42. Recycled hydrotalcite washed with 5 mL ethanol to remove organic impurities if any. Mg^{II} hydrotalcite catalyst can be readily recovered and reused for at least four runs without any significant loss of activity. XRD data of recovered hydrotalcite (Fig. 2) which showed the similar profile as fresh catalyst which confirmed that layered structure of hydrotalcite was maintained after the reaction.

2.2. Catalytic activity of hydrotalcite

By exploring the synthesis of coumarin derivatives the catalytic activity has been observed, results are incorporated in Table 4.

Table 3
Effect of metal composition of hydrotalcite on yield of coumarin.[a]

Entry	Ratio of hydrotalcite	Time (min)	Yield (%)
1	(2:1) Mg–Al-CO_3	70	84
2	(3:1) Mg–Al-CO_3	30	97
3	(4:1) Mg–Al-CO_3	70	79
4	(2:1) Ca–Al-CO_3	80	74
5	(3:1) Ca–Al-CO_3	60	90
6	(4:1) Ca–Al-CO_3	90	78
7	MgO	150	21
8	CaO	180	15

[a] Reaction conditions: solvent free conditions, heating at 70 °C.

Table 4
Catalytic activity of hydrotalcite for synthesis of coumarin derivatives.[a]

Product	Phenol	Mp. (°C)[c]	Mg–Al-CO_3 Time (min)	Hydrotalcite Yield (%)[b]	Ca–Al-CO_3 Time (min)	Hydrotalcite Yield (%)[b]
1a	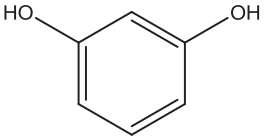	182–183	30	97	60	90
1b	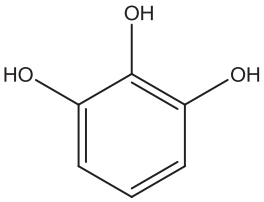	238–239	40	92	45	85
1c	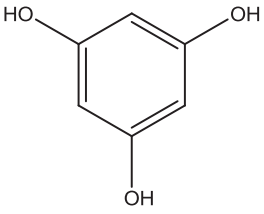	282–283	35	89	50	88
1d	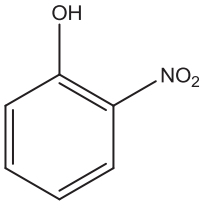	180–181	35	91	55	86
1e	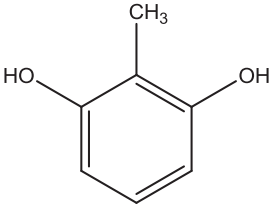	261–262	50	83	60	82
1f	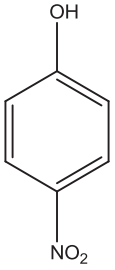	151–152	25	93	30	90
1g	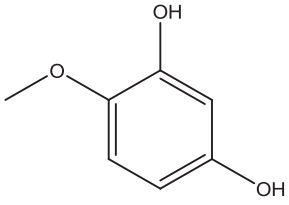	160–161	30	95	35	88

Table 4 (*Continued*)

Product	Phenol	Mp. (°C)[c]	Mg–Al-CO_3 Time (min)	Hydrotalcite Yield (%)[b]	Ca–Al-CO_3 Time (min)	Hydrotalcite Yield (%)[b]
2	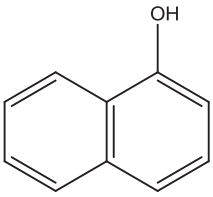	154–155	45	95	45	87

[a] Reaction was carried out using ethyl acetoacetate (0.0025 mol) and phenols (0.0025 mol) under solvent free conditions at 70 °C.
[b] Isolated yield.
[c] Melting point was uncorrected.

It shows that hydrotalcite (Mg–Al-CO_3) catalyzed the reaction efficiently with excellent yield and shorter time compared to Ca–Al-CO_3 type hydrotalcite. It has been previously suggested that although the basic site density decreases with increasing Al content the relative proportion of strongly basic site increases [36,37]. On the other hand, Since Al is more electronegative than Mg, an increase in Al should increase the average electronegativity of the catalyst and thus a decrease in the average electronic density of the unsaturated framework oxygens could be expected, with the corresponding effect on their basicity and catalytic activity [38–40]. As a result, the basicity and catalytic activity increased with elevating of Mg/Al molar ratio. However, when the Mg/Al molar ratio has exceeds 3.0, the catalytic activity decreases. It may be due to the formation of new weaker basic sites and thus decrease of strong basic site amount.

Methodology involves the reaction of phenols/naphthol (0.0025 mol) and ethyl acetoacetate (0.0025 mol) using hydrotalcite (Mg–Al-CO_3) as a catalyst under solvent free conditions at 70 °C (Scheme 1). Reaction was completed within few minutes with excellent yield (Table 5) and the synthesized compounds were characterized by comparing the observed spectral data and physical properties with those of authentic samples [10,16]. A variety of electron donating and electron withdrawing groups on phenol have been studied by preparing coumarin derivatives. There is no significant effect of electron donating and electron withdrawing subsituents on yield and time and resultant yield was obtained between ranges 82 and 97% within time range 30 and 50 min.

2.3. Basicity of hydrotalcite

Basicity of the catalyst was determined using Hammett indicator and benzoic acid titration method [41–43]. In this, 25 mg of the calcined catalyst was shaken with 1 mL solution of Hammett indicator in methanol and left to equilibrate. Color of catalyst was noted. The base strength is quoted as being stronger than weakest indicator which exhibits a color change. In benzoic acid titration method, 0.1 g of catalyst was suspended in 2 mL of phenolphthalein indicator solution (0.01 mg/mL toluene). It was then stirrer for 0.5 h and titrated against 0.01 M benzoic acid in toluene solution until pink color change to colorless. The total basicity was, thus determined.

All samples prepared in our study had the basic strength in the range of 9.3–15.0. The basicity of the catalysts with different Mg/Al molar ratios was shown in Fig. 3. The main basic sites with H_- in the range of 7.2–9.8 and the other sites with H_- in the range of 9.8–15.0 were observed, thus suggesting the calcined hydrotalcites contain different types of surface basic sites. Di Cosimo et al. [44] suggested that pure MgO possesses strong basic sites consisting predominantly of O^{2-} and calcined hydrotalcites contain surface basic sites. Our experimental results on the Hammett titration method consistent with this viewpoint. It indicates a wide basic site distribution as far as the basicity is concerned.

The total basicity of the hydrotalcite (catalyst) was increased gradually with the Mg/Al molar ratio and reach up to the maximum value at the Mg/Al molar ratio of 3.0. But basicity was decreased when further increase the molar ratio of Mg/Al, which resulted in a loss of the catalytic activity. Qualitatively similar trends were also reported by other researchers [37,45]. Nakatsuka et al. [37] found that the basicity measured by titration with benzoic acid reached a maximum for Mg/Al ratio of about 2.6. Also, Fishel and Davis [45] measured the number of basic sites by TPD of CO_2 and a maximum of the basic site density was observed at Mg/Al ratio of 3.0.

Best results were obtained with 3.0 HT, therefore basicity of 3.0 HT calcined at different temperatures was measured with the same method; the results are illustrated in Fig. 4. From this figure, it can be seen that the maximum basicity (reaching 3.6 mmol/g) is found at a calcinations temperature of 750 K and a low level of basicity is observed below 573 K and above 750 K. The increased

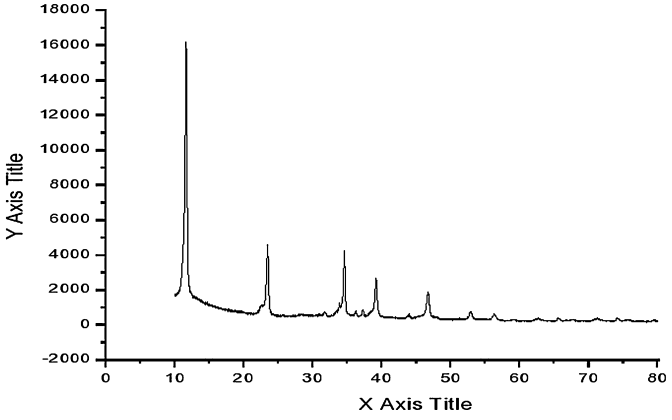

Fig. 2. XRD pattern of recovered hydrotalcite.

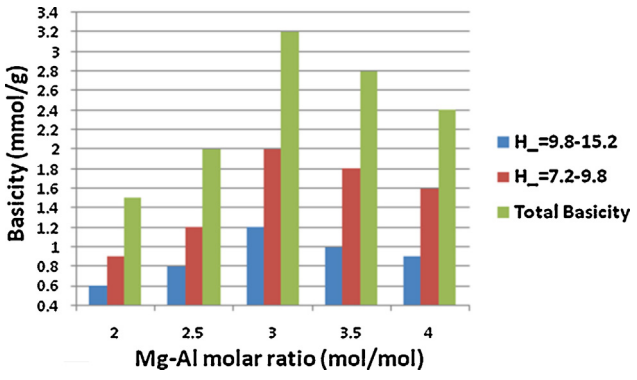

Fig. 3. Basicity of calcined hydrotalcite with different metal ratios.

Table 5
Hydrotalcite (Mg–Al-HT) catalyzed synthesis of coumarin derivatives.

Entry	Products	Phenol	Yield (%)[a]	Time (min)	Mp. (°C)[b] Found/Reported [Ref.]
1	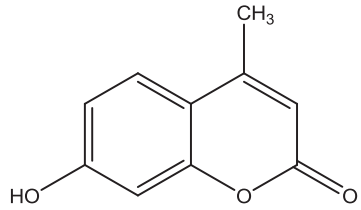 **1a**	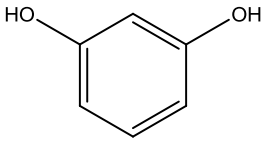	97	30	182–183/184–186 [10]
2	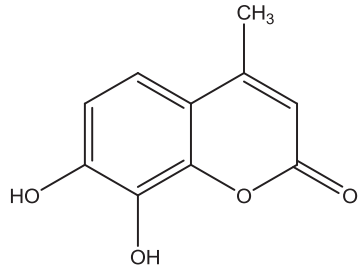 **1b**	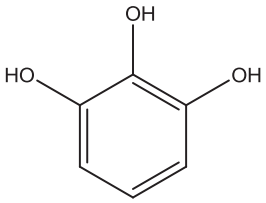	92	40	238–239/241–243 [55]
3	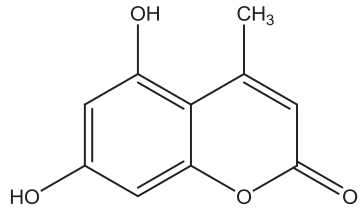 **1c**	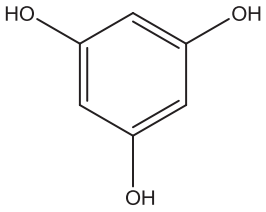	89	35	282–283/280–281 [55]
4	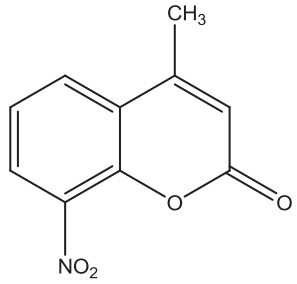 **1d**	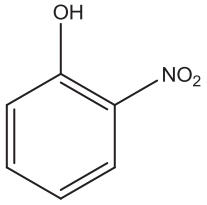	91	35	180–181/183–185 [16]
5	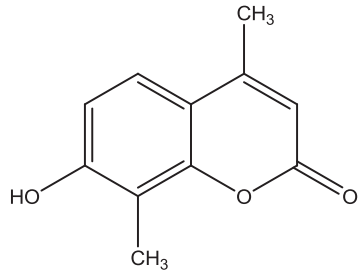 **1e**	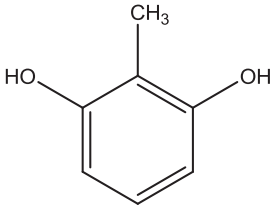	83	50	261–262/263–265 [11]
6	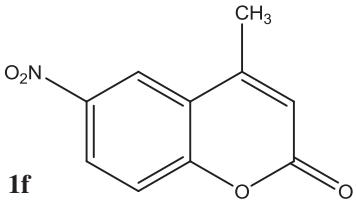 **1f**	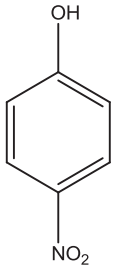	93	25	151–152/151–154 [16]

Table 5 (*Continued*)

Entry	Products	Phenol	Yield (%)[a]	Time (min)	Mp. (°C)[b] Found/Reported [Ref.]
7	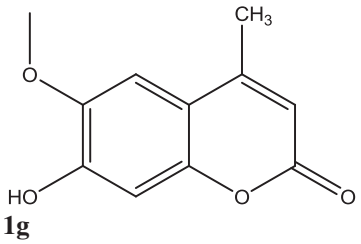 **1g**	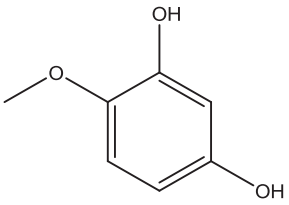	95	30	160–161/163–164 [16]
8	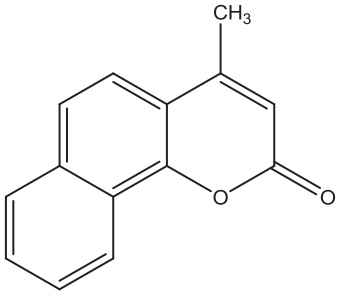	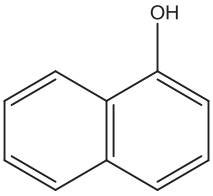	95	45	154–155/155–157 [10]

[a] Isolated yield
[b] Melting point was uncorrected

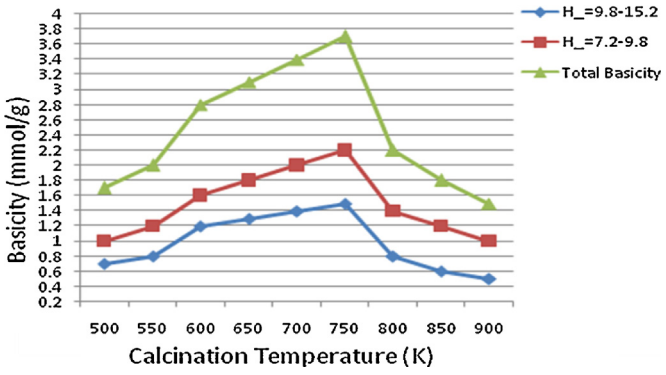

Fig. 4. Basicity of 3.0 hydrotalcite at different temperature.

basicity could be expected to correlate with an increase of the catalyst activity [46]. The thermal decomposition of Mg–Al-HT at about 750 K gives rise to mixed oxides whose X-ray diffraction patterns indicate a diffuse MgO-type structure with no segregate crystalline phases [38,47]. The first one, below 500 K, is attributed to the loss of interlayer water and the second, between 500 K and 750 K, to dehydroxylation and loss of the charge compensating anions [45,48,49]. The acid–base properties and, as a consequence, the catalytic activity of these Mg–Al-HT depend on chemical composition and on the conditions of the thermal treatment used to decompose the hydrotalcite precursor, 723–800 K being the range that produce the most active mixed oxides. Thus present studies have also been demonstrated the similar results which are supported by above literature.

2.4. Effect of aging time and catalytic activities

The SEM images of hydrotalcite samples at Mg/Al molar ratio of 3.0 were recorded to observe the effect of aging time on the morphology of the material. The micrographs at different aging times are shown in Fig. 5. From the micrographs of hydrotalcite, a well-developed layered and platelet structure of the hydrotalcite was observed. However, a spongy type structure is exhibited due to overlapping of such platelets. The SEM images of the hydrotalcite

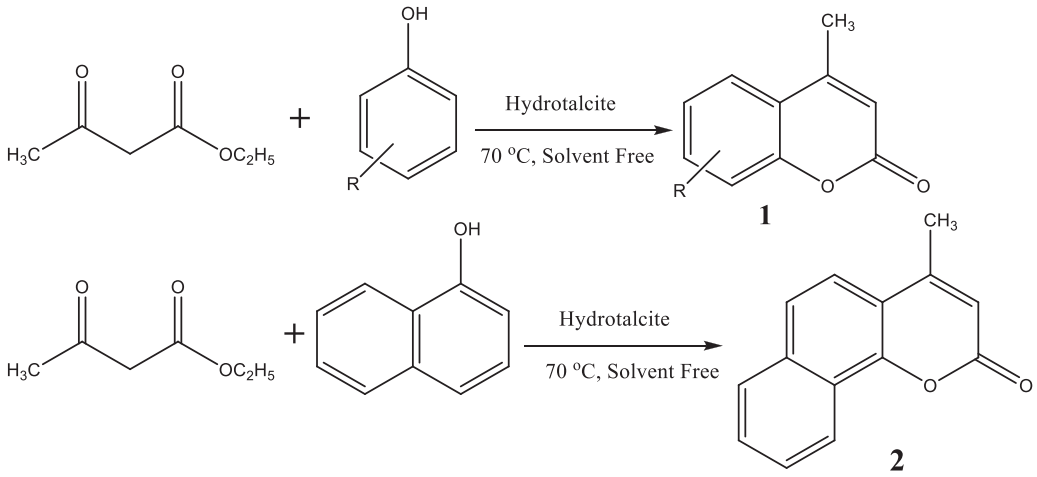

Scheme 1. Preparation of coumarin derivatives.

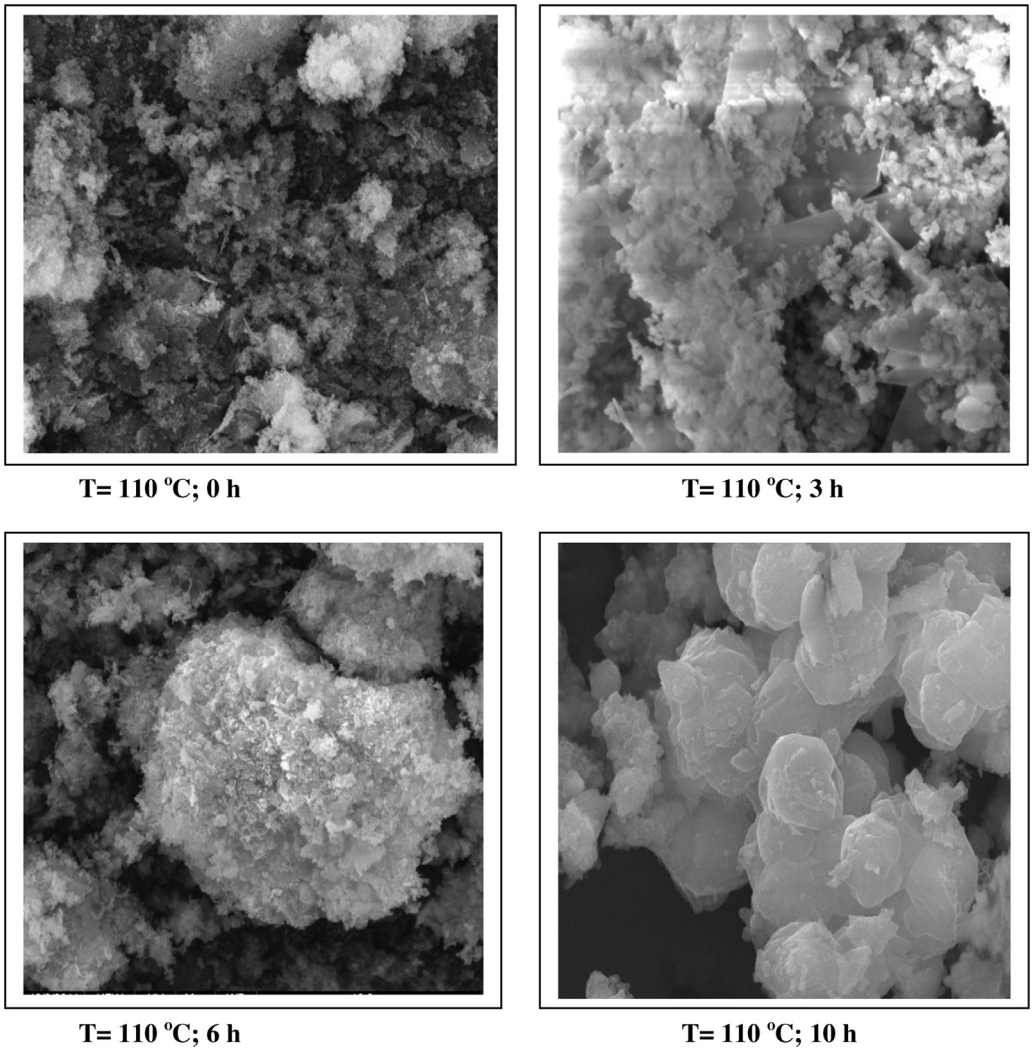

Fig. 5. SEM image of hydrotalcite at a Mg/Al (3:1) at different aging time at 110 °C.

showed a gradual crystallization during the hydrothermal treatment conditions. The crystallinity of the hydrotalcite was observed to be very poor at 0 h aging time and 110 °C hydrothermal treatment temperature; however, as aging time increases from 0 to 10 h, the crystallinity of the hydrotalcite also increased. These results confirmed an increase in the crystallinity of the hydrotalcite samples at Mg/Al under hydrothermal treatment conditions.

2.5. Characterization of hydrotalcite

Mg:Al atomic ratio was measured using X-ray microanalysis and found 3.16, which is in good agreement with the metallic ratio (3.0) taken in solution. The value of x [$x = M^{III}/M^{II} + M^{III}$] was found to 0.24, which suggest the purity of hydrotalcite [50]. Powder X-ray diffraction (P-XRD) pattern for sample Mg–Al-CO_3 is shown in Fig. 6. The presence of CO_3^{2-} anion in the interlayer gallery of the hydrotalcite is confirmed by the characteristic basal spacing d_{003} = 7.76 Å. This indicates a gallery height of 2.96 Å (assuming a thickness of 4.8 Å for the cationic sheets). The material is reasonably crystalline and suggests a relatively well-ordered sheet arrangement [51]. Diffraction peaks of the (0 0 3) basal plane that gives the distance between the layers became sharper which indicates higher crystallinity and order. This fact is supported by the increase in the ratio of the intensities of the diffraction from the (0 0 6) basal plane to that of the (0 0 3) one. The crystallite size of this sample was found 24.87 nm as calculated using Scherrer formula [52]. More intensive and sharper reflections of the (0 0 3) and (0 0 6) planes has found at low 2θ values (11–23°). A typical SEM image of Mg–Al-CO_3 hydrotalcite is shown in Fig. 6. This figure indicates the existence of lamellar particles looks like rounded hexagonal shape and typical of hydrotalcite like material. The material was found mesoporous with the surface area 90 m^2/g.

The Ca:Al metal ratio was found in good agreement with the initially taken metallic ratio. The observed value for Ca–Al-CO_3 was 3:2:1. The P-XRD patterns for the LDHs Ca–Al-CO_3 exhibits features commonly shown by layered materials. There are narrow, symmetric, strong lines at low 2θ values and weaker, less symmetric lines at high 2θ value (Fig. 7) [53]. Presence of CO_3^{2-} anion in the interlayer gallery of the hydrotalcite is confirmed by the characteristic basal spacing d_{003} = 3.38 Å. The lattice parameters a and c were calculated assuming 3R packing of the layers and from the positions of doublet corresponding to plane 1 1 0 and 1 1 3, 0 0 3, 0 0 6, 0 0 9 reflections. Sharp intense peaks at low diffraction angles (peaks close to 2θ = 11°, 24°, and 35°; ascribed to diffraction by basal planes (0 0 3), (0 0 6), and (0 0 9), respectively) and broad, less intense peaks at higher angles (peaks close to 2θ = 38°, 46°, and 60°); ascribed to diffraction by (1 0 5), (1 0 8) and (1 1 0) planes confirm the presence of hydrotalcite. The crystallite size of this sample was found 47.025 nm. The crystallographic parameter 'a' equals the average cation–cation distance in the brucite like

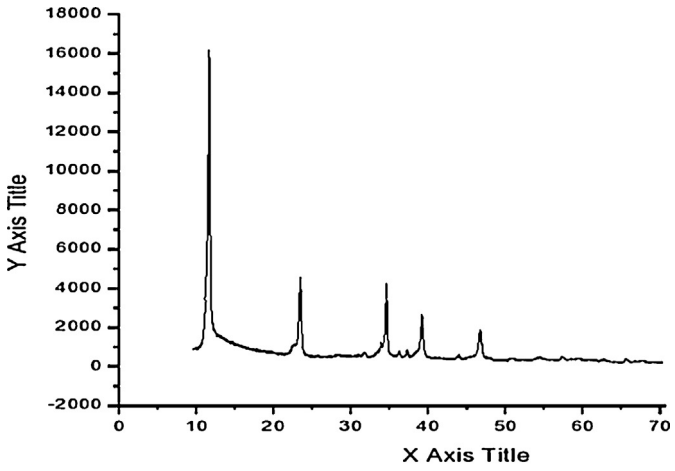

XRD Pattern Mg-Al- 3:1

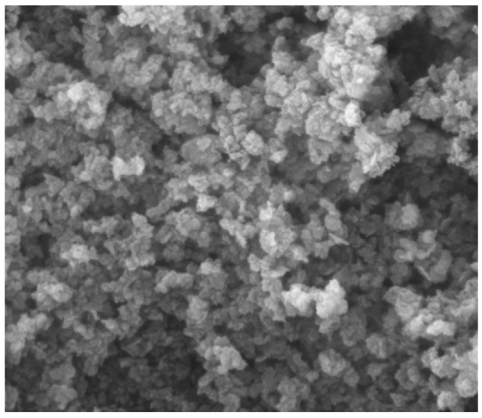

SEM Image Mg-Al- 3:1

Fig. 6. P-XRD pattern and SEM image of hydrotalcite (Mg–Al 3:1).

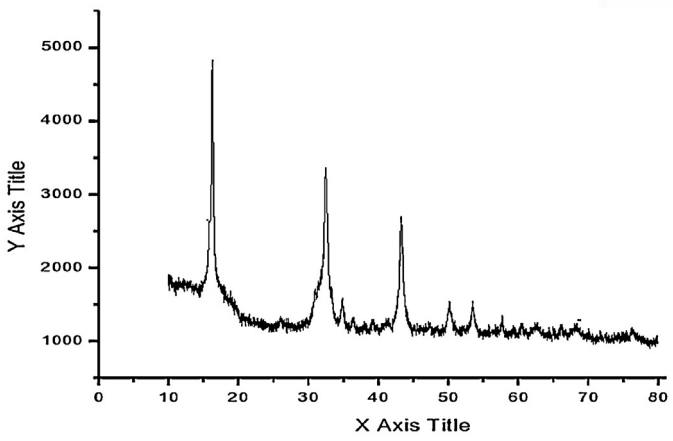

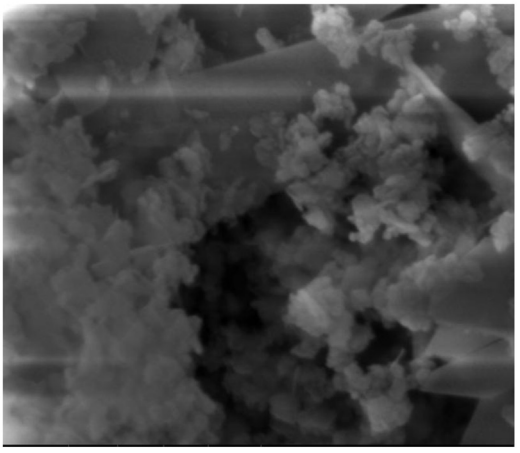

SEM Image (Ca-Al- 3:1)

Fig. 7. P-XRD and pattern and SEM image of hydrotalcite (Ca–Al 3:1).

layers, while parameter '*c*' is three times the distance from the center of one layer to the next and is controlled mostly by the size and orientation of the interlayer anion and the electrostatic forces operating between the interlayer anion and the layers. SEM (Fig. 7) of the material shows high crystallinity. The particles of hydrotalcite Ca–Al-CO_3 clearly exhibit the hexagonal shape; however, big needle shape particles are also visible.

2.6. Plausible mechanism

A plausible mechanism for formation of product 1 shown in Scheme 2. It is suggested that the lone pair of electrons of the phenolic OH group attacks at the carbonyl carbon of ethoxy moiety of ester (ethyl acetoester) with the elimination of alcohol molecule to give intermediate **A**. The intermediate **A** undergoes ring closure through electrophilic attack of the π-electrons at the activated

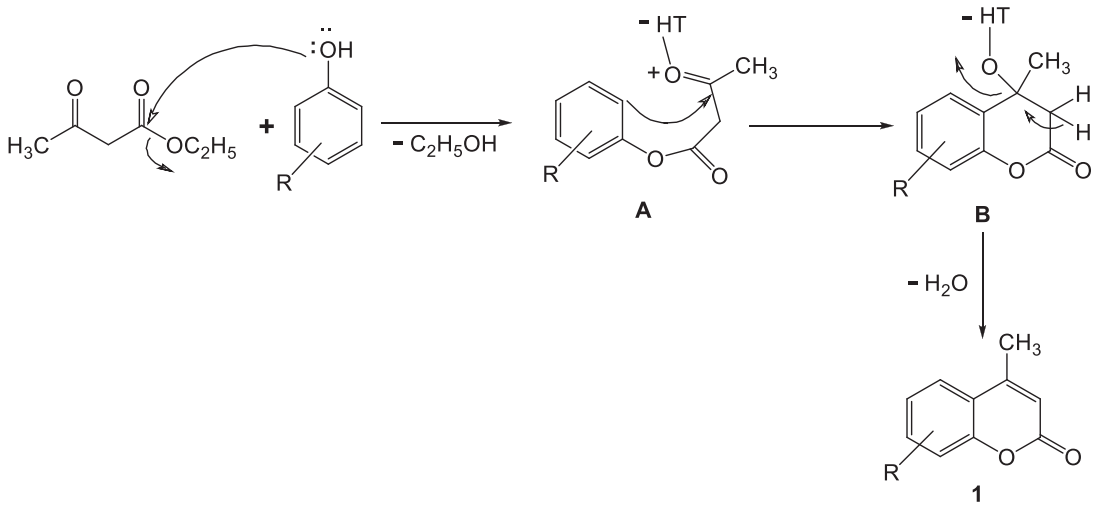

Scheme 2. Plausible reaction mechanism.

carbonyl carbon by active metal center of hydrotalcite to form intermediate **B**. The intermediate B then undergoes elimination of one water molecule to give target product **1**.

3. Conclusion

It can be concluded that synthesis coumarin derivatives have been developed using hydrotalcite (Mg–Al-CO_3), reusability of catalyst and ease of work-up make the method advantageous. The catalytic activities of the calcined hydrotalcite show a striking correlation with their corresponding basic properties and composition of metal content affected the yield of target molecules. The prepared catalyst were characterized with Hammett indicator-benzene carboxylic acid titration, SEM and XRD showing the strong basic sites in double layers and coordinatively unsaturated O^{2-} ion acting as basic sites in the calcined hydrotalcite may be responsible for their catalytic activity. The crystallization of hydraotalcite was significantly affected by hydrothermal treatment temperature and time. Conversion of reactant depends on the number of factors such as molar ratios of metal ions, calcination temperature, and crystallinity depends on the aging time. The crystallization of hydrotalcite (Mg/Al molar ratio = 3.0) was significantly affected by the aging time (0–10 h). This is first attempt to synthesize the coumarin derivatives using heterogeneous catalyst (hydrotalcite). The main advantages of this methodology are the short reaction times, simple catalyst system, higher yields, higher catalytic activity, solvent free conditions and good reusability.

4. Experimental

4.1. General

The ^{1}H NMR spectra were measured by BRUKER AVANCE II 400 NMR spectrometer with tretramethylsilane as an internal standard at 20–25 °C; data for ^{1}H NMR are reported as follow: chemical shift (ppm), integration, multiplicity (s, singlet; d, doublet; t, triplet; q, quartet; m, multiplet and br, broad), coupling constant (Hz). IR spectra were recorded by SHIMADZU, IR spectrometer of sample dispersed in KBr pellet and are reported in terms of frequency of absorption (cm^{-1}). Elemental analysis was performed by a Carlo-Erba EA1110 CNNO-S analyzer. E-Merck pre-coated TLC plates, RANKEM silica gel G for preparative thin-layer chromatography were used. Melting points were determined on electrical melting point apparatus in open capillary and were uncorrected. Phenol, naphthol and ethyl acetoacetate were purchased from Himedia, Mumbai India and used without any purification.

4.2. Preparation of hydrotalcite

The catalyst hydrotalcite was synthesized using literature procedure [54].

Typical procedure. Mixed salt solutions containing Ca^{2+}/Mg^{2+} and Al^{3+} in molar ratios of 3:1 were taken. *p*H of the solution was raised to 8.5 using 25% NH_4OH. The thick white slurry was aged and autogenous pressure in an autoclave to achieve small particle size and high surface area. The precipitate was filtered ad washed with deionized water and dried at 110 °C.

4.3. One-pot three component reaction

Typical procedure for synthesis of coumarin. A mixture of phenols (0.0025 mol) and dicarbonyl (0.0025 mol) were heated at 70 °C under solvent free conditions using hydrotalcite (Mg–Al-CO_3, 50 mg) as a catalyst. The time taken by different phenols in reaction was as mentioned in Table 4. After completion of the reaction (TLC analysis using ethyl acetate:petroleum ether, 1:3), the reaction mixture was cooled to room temperature and poured in cold water. The solid mass was filtered. It was dissolved in ethanol and filtered. The solid hydrotalcite got separated as solid. The filtrate having product soluble in ethanol was concentrate to crystallize the product. Hydrotalcite was washed with ethanol to remove organic impurity.

4.4. Compound **1a**

White powder, mp. 182–183 °C; IR (KBr) (υ_{max}, cm^{-1}): 3260 (OH_{str}), 3080 (C—H_{str}), 1690 (C=O_{str}). ^{1}H NMR (400 MHz, $CDCl_3$): δ_H 2.65 (s, 3H, Me), 6.41 (s, 1H, C=CH), 6.64 (d, *J* = 8.4 Hz, 1H, ArH), 7.24 (s, 1H, ArH), 7.57 (d, *J* = 7.76 Hz, 1H, ArH), 8.9 (s, 1H, OH); ^{13}C NMR (100 MHz, $CDCl_3$): 23.09, 102.96, 111.80, 115.02, 131.95, 137.56, 153.46, 157.22, 162.27, 165.55; EIMS: *m*/*z*: Calculated for $C_{10}H_8O_3$ 176, Found $[M]^+$ 176; C, H and N analyses Calculated for C 68.18, H 4.54, Found C 68.25, H 4.59.

4.5. Compound **1b**

White solid, mp 238–239 °C; ^{1}H NMR (400 MHz; DMSO-d_6): δ_H 2.35 (s, 3H, Me), 6.30 (s, 1H, C=CH), 6.46 (d, *J* = 8.4 Hz, 1H, ArH), 7.20 (d, *J* = 8.4 Hz, 1H, ArH), 9.26 (s, 2H, OH); ^{13}C NMR (100 MHz, DMSO-d_6): 23.1, 110.7, 111.2, 111.5, 117.6, 133.4, 151.46, 152.6, 165.4; EIMS: *m*/*z*: Calculated for $C_{10}H_8O_4$ 192, Found $[M]^+$ 192; C, H and N analyses Calculated for C 62.50, H 4.20, Found C 62.63, H 4.39.

4.6. Compound **1c**

Colorless solid, mp 282–283 °C; ^{1}H NMR (400 MHz; DMSO-d_6): δ_H 2.47 (s, 3H, Me), 6.36 (s, 1H, C=CH), 6.89–6.92 (m, 2H, ArH), 9.82 (s, 1H, OH), 10.12 (s, 1H, OH); ^{13}C NMR (100 MHz, DMSO-d_6): 23.09, 102.9, 111.8, 115.0, 131.9, 137.5, 153.46, 157.22, 162.27, 165.55; EIMS: *m*/*z*: Calculated for $C_{10}H_8O_4$ 192, Found $[M]^+$ 192; C, H and N analyses Calculated for C 62.50, H 4.20, Found C 62.59, H 4.12.

4.7. Compound **1d**

Colorless solid, mp 180–181 °C; ^{1}H NMR (400 MHz; DMSO-d_6): δ_H 2.40 (s, 3H, Me), 6.33 (s, 1H, C=CH), 6.81–6.89 (m, 3H, ArH), 10.12 (s, 1H, OH); ^{13}C NMR (100 MHz, DMSO-d_6): 14.04, 23.1, 115.0, 116.0, 128.1, 151.23, 157.23, 162.99, 165.9, 171.8; EIMS: *m*/*z*: Calculated for $C_{10}H_7NO_4$ 205.17, Found $[M+H]^+$ 206; C, H and N analyses Calculated for C 58.54, H 3.44, N 6.83 Found C 58.41, H 3.59, N 6.88.

4.8. Compound **1e**

Colorless solid, mp 261–262 °C; ^{1}H NMR (400 MHz; DMSO-d_6): δ_H 2.11 (s, 3H, CH_3), 2.46 (s, 3H, Me), 6.39 (s, 1H, C=CH), 6.80 (d, *J* = 8.4 Hz, 1H, ArH), 7.41 (d, *J* = 8.4 Hz, 1H, ArH), 10.3 (brs, 1H); ^{13}C NMR (100 MHz, DMSO-d_6): 14.04, 23.11, 115.03, 116.07, 122.9, 151.3, 157.2, 162.9, 165.9, 171.8; EIMS: *m*/*z*: Calculated for $C_{11}H_{10}O_3$ 190.2, Found $[M]^+$ 190; C, H and N analyses Calculated for C 69.46, H 5.30, Found C 69.61, H 5.36.

4.9. Compound **1f**

White solid, mp 151–152 °C; ^{1}H NMR (400 MHz; DMSO-d_6): δ_H 2.40 (s, 3H, Me), 6.33 (s, 1H, C=CH), 6.61 (d, *J* = 8.4 Hz, 1H, ArH), 7.2 (s, 1H, ArH), 7.51 (d, *J* = 7.76 Hz, 1H, ArH), 10.12 (s, 1H, OH); ^{13}C NMR (100 MHz, DMSO-d_6): 23.09, 102.8, 110.8, 111.9, 115.1, 132.5, 137.6, 153.5, 162.3, 165.6; EIMS: *m*/*z*: Calculated for $C_{10}H_7NO_4$ 205.17, Found $[M+H]^+$ 206; C, H and N analyses Calculated for C 58.54, H 3.44, N 6.83 Found C 58.41, H 3.59, N 6.88.

4.10. Compound **1g**

White powder, mp 160–161 °C; ^{1}H NMR (400 MHz; DMSO-d_6): δ_H 2.46 (s, 3H, Me), 3.89 (s, 1H, OCH_3), 6.36 (s, 1H, C=CH), 6.80–6.91 (m, 2H, ArH), 9.82 (s, 1H, OH); ^{13}C NMR (100 MHz, DMSO-d_6): 23.7, 57.2, 103.2, 111.8, 113.9, 152.0, 154.5, 159.4, 163.2, 166.6; EIMS: *m/z*: Calculated for $C_{11}H_{10}O_3$ 206.19, Found $[M]^+$ 206; C, H and N analyses Calculated for C 64.07, H 4.89 Found C 64.19, H 5.03.

4.11. Compound **2**

White powder, mp 154–155 °C; IR (KBr) (υ_{max}, cm^{-1}): 1675 (C=O_{str}). ^{1}H NMR (400 MHz, $CDCl_3$): δ_H 2.71 (s, 3H, Me), 6.51 (s, 1H, C=CH), 7.03–7.63 (m, 6H, ArH); ^{13}C NMR (100 MHz, $CDCl_3$): 23.17, 102.56, 111.65, 122.22, 122.92, 123.68, 126.40, 126.79, 127.98, 137.43, 141.26, 154.04, 162.59, 165.44; EIMS: *m/z*: Calculated for $C_{14}H_{10}O_2$ 210, Found $[M]^+$ 210; C, H and N analyses Calculated for C 80.01, H 4.76, Found C 80.05, H 4.81.

Acknowledgements

We are grateful thanks to Dr. Yogesh Sharma, Water India Ltd., Delhi and SIAF Facility, Punjab University, Chandigarh for spectral analytical data.

References

[1] (a) I. Kostova, Curr. Med. Chem. 5 (2005) 29;
(b) F. Borges, F. Roleira, N. Milhazes, L. Santana, E. Uriarte, Curr. Med. Chem. 12 (2005) 887;
(c) J.M. Schmidt, G.B. Tremblay, M. Page, J. Mercure, M. Feher, R. Dunn-Dufault, M.G. Peter, P.R. Redden, J. Med. Chem. 46 (2003) 1289;
(d) J. Pandey, A.K. Jha, K. Hajela, Bioorg. Med. Chem. 12 (2004) 2239;
(e) J.M. Sayer, Y. Haruhiko, A.W. Wood, A.H. Conney, D.M. Jerina, J. Am. Chem. Soc. 104 (1982) 5562;
(f) Y.A.G.P. Gunawardana, N.S. Kumar, M.U.S. Sultanbawa, Phytochemistry 18 (1979) 1017;
(g) B.I. Alo, A. Kandil, P.A. Patil, M.J. Sharp, M.A. Snieckus, V. Siddiqui, J. Org. Chem. 56 (1991), and Refs. 6–10 cited therein 3763.
[2] H.W.T. Sidwell, L. Fritz, C. Tamm, Helv. Chim. Acta 54 (1971) 207.
[3] C. Tamm, Arzneim. -Forsch. 22 (1972) 1776.
[4] H. Raistrick, C.E. Stilkings, R. Thomas, Biochemistry 55 (1953) 421.
[5] R.W. Pero, D. Harvan, M.C. Blois, Tetrahedron Lett. 14 (1973) 945.
[6] W. Steglich, B. Fugmann, S. Lang-Fugmann, ROMPP Encyclopedia of Natural Products, B. Eds.; Thieme: Stuttgart, (1997).
[7] S. Frere, V. Thiery, T. Besson, Tetrahedron Lett. 42 (2001) 2791.
[8] S.P. Chavan, K. Shivasankar, R. Sivappa, R. Kale, Tetrahedron Lett. 43 (2002) 8583.
[9] S.D. Bose, A.P. Rudradas, M.H. Babu, Tetrahedron Lett. 43 (2002) 9195.
[10] H. Valizadeha, A. Shockravi, Tetrahedron Lett. 46 (2005) 3501.
[11] G.V.M. Sharma, J.J. Reddy, P.S. Lakshmi, P.R. Krishna, Tetrahedron Lett. 46 (2005) 19.
[12] J.C. Rodríguez-Domínguez, G. Kirsch, Tetrahedron Lett. 47 (2006) 3279.
[13] M.K. Potdar, S.S. Mohile, M.M. Salunkhe, Tetrahedron Lett. 42 (2001) 9285.
[14] V.M. Alexander, R.P. Bhat, S.D. Saman, Tetrahedron Lett. 46 (2005) 6957.
[15] G.P. Romanelli, D. Bennardi, D.M. Ruiz, G. Baronetti, H.J. Thomas, J.C. Autino, Tetrahedron Lett. 45 (2004) 8935.
[16] S.S. Bahekara, D.B. Shinde, Tetrahedron Lett. 45 (2004) 7999.
[17] J. Li, H. Chen, D.Z. Negrerie, Y. Du, K. Zhao, RSC Adv. 3 (2013) 4311.
[18] R.K. Verma, G.K. Verma, G. Shukla, M.S. Singh, RSC Adv. 2 (2012) 2413.
[19] M. Maheswara, V. Siddaiah, G.L.V. Damu, Y.K. Rao, C.V. Rao, J. Mol. Catal. A: Chem. 255 (2006) 49.
[20] K.C. Majumdar, S. Samanta, I. Ansary, B. Roy, RSC Adv. 2 (2012) 2137.
[21] (a) M. Matzke, S. Stolte, K. Thiele, T. Juffernholz, J. Arning, J. Ranke, U. Welzbiermann, B. Jastorff, Green Chem. 9 (2007) 1198;
(b) D. Kralisch, A. Stark, S. Korsten, G. Kreisel, B. Ondruschka, Green Chem. 7 (2005) 301;
(c) T. Pham, C. Cho, Y. Yun, Water Res. 44 (2010) 352.
[22] G. Centi, S. Perathoner, Microporous Mesoporous Mater. 107 (2008) 3.
[23] S.K. Sharma, P.A. Parikh, R.V. Jarra, J. Mol. Catal. A: Chem. 278 (2007) 135.
[24] C.M. Jinesh, C.A. Antonyraj, S. Kannan, Catal. Today 141 (2009) 176.
[25] (a) A. Corma, S. Iborra, S.S. Miquel, J. Primo, J. Catal. 173 (1998) 315;
(b) K. Motocura, N. Fujita, K. Mori, T. Mizugaki, K. Ebitani, K. Htsukawa, K. Kanedar, Chem. Eur. J. 12 (2006) 8228.
[26] M. Turco, G. Bagnasco, U. Costantino, F. Marmottini, T. Montanari, G. Ramis, G. Busca, J. Catal. 228 (2004) 56.
[27] B.F. Sels, D.E. De Vos, P.A. Jacobs, Catal. Rev. Sci. Eng. 43 (2001) 443.
[28] Y. Xi, R.J. Davis, J. Catal. 254 (2008) 190.
[29] S.K. Yun, T.J. Pinnavaia, Chem. Mater. 7 (1995) 348.
[30] B.M. Choudary, M.L. Kantam, V. Neeraja, K.K. Rao, F. Figueras, L. Delmotte, Green Chem. 3 (2001) 257.
[31] (a) S.K. Sharma, P.A. Parikh, R.V. Jasra, J. Mol. Catal. A: Chem. 278 (2007) 135;
(b) V.R.L. Constantino, T. Pinnavaia, J. Inorg. Chem. 34 (1995) 883.
[32] (a) A. Corma, V. Fornes, R.M. Martinaranda, F. Rey, J. Catal. 134 (1992) 58;
(b) M.J. Climent, A. Corma, S. Iborra, J. Primo, J. Catal. 151 (1995) 60.
[33] C.O. Veloso, C.N. Perez, B.M. De Souza, E.C. Lima, A.G. Dias, J.L.F. Monteiro, C.A. Henriques, Microporous Mesoporous Mater. 107 (2008) 23.
[34] W.L. Xie, H. Peng, L.G. Chen, J. Mol. Catal. A: Chem. 246 (2006) 24.
[35] V.K. Diez, C.R. Apesteguia, J.I. Di Cosimo, J. Catal. 215 (2003) 220.
[36] D. Tichit, M.H. Lhouty, A. Guida, B.H. Chiche, F. Figueras, A. Auroux, B. Bartalini, E. Garrone, J. Catal. 151 (1995) 1995.
[37] T. Nakatsuka, T.H. Kawasaki, S. Yamashita, S. Kohjiya, Bull. Chem. Soc. Jpn. 52 (1979) 2449.
[38] W.T. Reichle, S.Y. Kang, D.S. Everhardt, J. Catal. 101 (1986) 352.
[39] P. Mustrowski, L. Chmielarz, E. Bozek, M. Sawalha, F. Roessner, Mater. Res. Bull. 39 (2004) 263.
[40] J. Shen, M. Tu, C. Hu, J. Solid State Chem. 137 (1998) 295.
[41] D.G. Cantrell, L.J. Gillie, A.F. Lee, K. Wilson, Appl. Catal. A: Gen. 287 (2005) 183.
[42] J.M. Fraile, N. Garcia, J.A. Mayoral, E. Pires, L. Rodan, Appl. Catal. A: Gen. 364 (2009) 87.
[43] H.J. Hattori, Jpn. Petrol. Inst. 47 (2004) 67.
[44] J.J. Di Cosimo, V.K. Di'ez, M. Xu, E. Iglesia, C.R. Apesteguia, J. Catal. 178 (1998) 499.
[45] C.T. Fishel, R. Davis, Langmuir 10 (1994) 159.
[46] P. Kustrowski, D. Sulkowska, L. Chmielarz, R. Dziembaj, Appl. Catal. A: Gen. 302 (2006) 317.
[47] (a) A.L. McKenzie, C.T. Fishel, R.J. Davis, J. Catal. 138 (1992) 547;
(b) F. Rey, V. Fornés, J.M. Rojo, J. Chem. Soc.: Faraday Trans. 83 (1992) 2233.
[48] W.T. Reichle, Chemtech 16 (1986) 58.
[49] A. Takagaki, K. Iwatani, S. Nishimura, K. Ebitani, Green Chem. 12 (2010) 578.
[50] F. Cavani, F. Trifiro, A. Vaccari, Catal. Today 11 (1991) 173.
[51] F.M. Labojos, V. Rives, M.A. Ulibarri, J. Mater. Sci. 27 (1992) 1546.
[52] A.S. Bookin, A. Dritis, Clays Clay Miner. 41 (1993) 551.
[53] K.R. Kottapalli, G. Monique, S.V. Jaime, F. Francois, J. Catal. 173 (1998) 115.
[54] S. Gupta, D.D. Agarwal, S. Banerjee, Indian J. Chem.: Sect. A 47 (2008) 1004.
[55] L. Wang, J. Xia, H. Tian, C. Qian, Y. Ma, Indian J. Chem. 42B (2003) 2097.